Wideband generation of pulses in dual-pump optical parametric amplifier: theory and experiment

Mohammad Amin Shoaie,[1,*] Amirhossein Mohajerin-Ariaei,[2] Armand Vedadi,[1] and Camille-Sophie Brès[1]

[1]*Photonic Systems Laboratory (PHOSL), STI-IEL, Ecole Polytechnique Fédérale de Lausanne (EPFL), CH-1015 Lausanne, Switzerland*

[2]*Department of Electrical Engineering, University of Southern California, 3740 McClintock Ave, Los Angeles, California 90089, USA*

[*]*amin.shoaie@epfl.ch*

Abstract: The generation of pulses in dual-pump fiber optical parametric amplifier is investigated. Theoretically, it is shown that in an analogical manner to pulse generation in single-pump fiber optical parametric amplifiers, the generated pulse shape depends on the linear phase mismatch between the interacting waves. However the dual-pump architecture allows for the bounding of the phase mismatch over a wide bandwidth. This feature permits the generation of uniform pulses over a wide bandwidth, contrary to the single-pump architecture. Using the developed theory, a pulse source with uniform pulses at 5 GHz repetition rate and duty cycle of 0.265 over 40 nm is demonstrated.

OCIS codes: (060.4370) Nonlinear optics, fibers; (060.2320) Fiber optics amplifiers and oscillators

References and links

1. E. Yoshida, N. Shimizu, and M. Nakazawa, "A 40-GHz 0.9-ps regeneratively mode-locked fiber laser with a tuning range of 1530-1560 nm," IEEE Photonics Technol. Lett. **11**(12), 1587–1589 (1999).
2. A. O. Wiberg, C.-S. Brès, B.-P. Kuo, E. Myslivets, and S. Radic, "Cavity-less 40 GHz pulse source tunable over 95 nm" in *European Conference and Exhibition on Optical Communication ECOC 2009*, OSA Technical Digest (online) (Optical Society of America, 2009), pp. 1–2.
3. V. R. Supradeepa and A. M. Weiner, "Bandwidth scaling and spectral flatness enhancement of optical frequency combs from phase-modulated continuous-wave lasers using cascaded four-wave mixing," Opt. Lett. **37**(15), 3066–3068 (2012).
4. X. Wang, Y. Zhou, X. Xu, C. Zhang, J. Xu, and K. K. Y. Wong, "Multiwavelength Pulse Generation Using Fiber Optical Parametric Oscillator," IEEE Photonics Technol. Lett. **25**(1), 33–35 (2013).
5. M. E. Marhic, *Fiber Optical Parametric Amplifiers, Oscillators and Related Devices* (Cambridge University, 2008).
6. C. Yu, T. Luo, B. Zhang, Z. Pan, M. Adler, Y. Wang, J. E. McGeehan, and A. E. Willner, "Wavelength-shift-free 3R regenerator for 40-Gb/s RZ system by optical parametric amplification in fiber," IEEE Photonics Technol. Lett. **18**(24), 2569–2571 (2006).
7. J. Li, J. Hansryd, P. O. Hedekvist, P. A. Andrekson, and S. N. Knudsen, "300-Gb/s eye-diagram measurement by optical sampling using fiber-based parametric amplification," IEEE Photonics Technol. Lett. **13**(9), 987–989 (2001).
8. G.-W. Lu, K. Abedin, T. Miyazaki, and M. Marhic, "RZ-DPSK OTDM demultiplexing using fibre optical parametric amplifier with clock-modulated pump," IEE Electron. Lett. **45**(4), 221–222 (2009).
9. T. Torounidis, M. Karlsson, and P. A. Andrekson, "Fiber optical parametric amplifier pulse source: Theory and experiments," J. Lightwave Technol. **23**(12), 4067–4073 (2005).
10. A. Vedadi, A. M. Ariaei, M. M. Jadidi, and J. A. Salehi, "Theoretical study of high repetition rate short pulse generation with fiber optical parametric amplification," J. Lightwave Technol. **30**(9), 1263–1268 (2012).
11. A. Vedadi, M. A. Shoaie, and C. S. Brès, "Near-Nyquist optical pulse generation with fiber optical parametric amplification," Opt. Express **20**(26), B558–B565 (2012).
12. C. J. McKinstrie, S. Radic, and A. Chraplyvy, "Parametric amplifiers driven by two pump waves," IEEE J. Sel. Top. Quantum Electron. **8**(3), 538–547 (2002).

#202294 - $15.00 USD Received 4 Dec 2013; revised 11 Feb 2014; accepted 12 Feb 2014; published 20 Feb 2014

13. M. Yu, C. J. McKinstrie, and G. P. Agrawal, "Instability due to cross-phase modulation in the normal-dispersion regime," Phys. Rev. E Stat. Phys. Plasmas Fluids Relat. Interdiscip. Topics **48**(3), 2178–2186 (1993).
14. A. A. Vedadi, M. A. Shoaie, and C.-S. Brès, "Experimental investigation of pulse generation with one-pump fiber optical parametric amplification," Opt. Express **20**(24), 27344–27354 (2012).
15. M. E. Marhic, Y. Park, F. S. Yang, and L. G. Kazovsky, "Broadband fiber-optical parametric amplifiers and wavelength converters with low-ripple Chebyshev gain spectra," Opt. Lett. **21**(17), 1354–1356 (1996).
16. A. Vedadi, C. S. Brès, and M. A. Shoaie, "Wideband uniform generation of shape-adjustable pulses in two-pump fiber optic parametric amplifier," in *European Conference and Exhibition on Optical Communication ECOC 2013*, OSA Technical Digest (online) (Optical Society of America, 2013), pp. 873–875.
17. A. A. Vedadi, N. Grossard, J. Hauden, E. Lantz, H. Maillotte, and T. Sylvestre, "Demonstration of an integrated $LiNbO_3$ synchronized double phase modulator and its application to dual-pump fiber optical parametric amplifiers and wavelength converters," J. Lightwave Technol. **26**(7), 777–781 (2008).
18. M. C. Ho, M. E. Marhic, K. Y. K. Wong, and L. G. Kazovsky, "Narrow-linewidth idler generation in fiber four-wave mixing and parametric amplification by dithering two pumps in opposition of phase," J. Lightwave Technol. **20**(3), 469–476 (2002).
19. J. Hansryd and P. Andrekson, "Wavelength tunable 40GHz pulse source based on fibre optical parametric amplifier," IEE Electron. Lett. **37**(9), 584–585 (2001).
20. F. Yaman, Q. Lin, G. P. Agrawal, and S. Radic, "Pump-noise transfer in dual-pump fiber-optic parametric amplifiers: Walk-off effects," Opt. Lett. **30**(9), 1048–1050 (2005).
21. A. Bogris, D. Syvridis, P. Kylemark, and P. A. Andrekson, "Noise characteristics of dual-pump fiber-optic parametric amplifiers," J. Lightwave Technol. **23**(9), 2788–2795 (2005).
22. P. Kylemark, J. Ren, M. Karlsson, S. Radic, C. J. McKinstrie, and P. A. Andrekson, "Noise in dual-pumped fiber-optical parametric amplifiers: Theory and experiments," J. Lightwave Technol. **25**(9), 2837–2846 (2007).
23. J. M. Chavez Boggio, J. D. Marconi, S. R. Bickham, and H. L. Fragnito, "Spectrally flat and broadband double-pumped fiber optical parametric amplifiers," Opt. Express **15**(9), 5288–5309 (2007).

1. Introduction

Optical short pulse generation has been subject to a great interest due to its many applications in medical imaging, microscopy, spectroscopy as well as optical communication. One commonly used short pulse source is the modelocked laser (MLL). Although various MLLs with remarkable performance in terms of amplitude and phase jitter have been realized [1], their strict phase-locking constraint results in non-trivial operation as well as high sensitivity to external perturbation. Moreover, not only is the repetition rate dictated by the cavity mode spacing, but also the lasing bandwidth limits the pulse duration as well as operational wavelength. An alternative approach to the generation of optical short pulses is to rely on a cavity-less source. The single pass structure of such pulse source leads to less sensitivity toward environmental fluctuations. It also allows for the sweeping of the repetition rate over some range without the need for tuning the cavity correspondingly. Wavelength tunability can also be achieved. In [2] a stable 40 GHz cavity-less pulse source based on linear pulse compression in a dispersion-flattened dispersion compensating fiber (DF-DCF) was demonstrated reaching a 95 nm bandwidth tunability.

Another approach to generate pulses on a cavity-less all-fiber architecture is to exploit the quasi-instantaneous response of the Kerr effect in highly nonlinear fibers (HNLF). Indeed, using the four-wave mixing process (FWM), different pulse sources with interesting features such as high repetition rate [3], flat frequency comb [3] or multi-wavelength generation [4] were demonstrated. Among these approaches, fiber optical parametric amplifiers (FOPA) are of particular interest. FOPA is based on FWM in which the dispersion of the amplifying waveguide was designed so that an efficient transfer of energy takes place from one or two pump wave(s) to a signal wave and a generated idler. It is an energy conserving process and its efficiency is based on phase matching between the interacting waves [5]. FOPAs have widely been used to generate optical pulses; moreover they allow for the generation of optical time windows that have been applied for optical regeneration [6], optical sampling [7] and demultiplexing [8].

Although most studies on short pulse generation in single-pump FOPA with a sinusoidal modulated pump were focused on the exponential gain region [9], it has been shown that the generated pulse shape and pulse duration depend on the signal frequency relative to the pump frequency [10]. In particular, operating at one of the extremities of the gain spectrum

#202294 - $15.00 USD Received 4 Dec 2013; revised 11 Feb 2014; accepted 12 Feb 2014; published 20 Feb 2014

associated with the pump peak power generates the shortest pulses with a near-sinc shape [11]. While it is possible to tune the wavelength of the generated pulse by simultaneously adjusting pump and signal wavelengths, the pulse amplitude and width will vary with its frequency detuning from a fixed pump position. As a result temporal dynamics for pulse generation in single-pump FOPA is limited to a very narrow bandwidth at any spectral gain region.

In this paper we study the theory of short pulse generation in a dual-pump FOPA and demonstrate that by taking advantage of phase-matching bounding, it is possible to generate an identical temporal window over an extended frequency range. As a proof of concept we experimentally demonstrate the generation of identical pulses based on a dual-pump FOPA where both pumps are modulated simultaneously. The remainder of the paper is organized as follows. In section 2 by introducing the gain sensitivity, it is shown how a small decrease of one or both of the pumps powers from their peaks induces an abrupt decrease of the idler power that depends on the phase matching and leads to the generation of pulses. By highlighting that the linear phase mismatch can be bound to any desired value, it is shown that uniform pulses can be generated over a wide bandwidth. In section 3, we present an experimental demonstration of uniform pulse generation over a wide bandwidth based on dual-pump FOPA. Discussion and conclusion are provided in section 4.

2. Theoretical analysis

2.1 Gain sensitivity

In this section, we introduce, in a similar manner as in [10], the concept of gain sensitivity and highlight its impact on pulse generation in dual-pump FOPAs.

Dual-pump parametric amplification in a silica fiber is based on non-degenerate FWM whereby two high power pumps at angular frequencies ω_{P1} and ω_{P2} are launched into a highly nonlinear fiber (HNLF) together with a signal at ω_s, which is assumed to be located in the inner band of the two pumps. When the signal is located far from the pumps, FWM satisfying energy conservation condition $\omega_{P1} + \omega_{P2} = \omega_s + \omega_i$, where ω_i is the idler frequency, is sufficient to model the output optical gain spectrum. This model is referred to as the two-sideband (TS) interaction model. When the signal is located close to either of the pumps, the TS model is no longer applicable and one must include the two generated outer sidebands to correctly predict the gain behavior [12, 13]. This latter model is referred to as the four-sideband (FS) model and its solutions have to be calculated numerically.

The efficiency of the energy transfer from the pumps to signal and idler through that FWM process depends on the phase-matching condition between the signal, idler and the two pumps. Assuming scalar waves, no pump depletion and neglecting loss, one can write the idler gain G_i and signal power gain G_s according to the TS interaction model as [5]:

$$G_i = \left(\frac{r}{g} \sin \mathrm{h}(gL) \right)^2 \tag{1a}$$

$$G_s = G_i + 1 \tag{1b}$$

where r and the parametric gain coefficient g are given by:

$$r = 2\gamma \sqrt{P_1 P_2} \tag{2}$$

$$g^2 = r^2 - \left(\kappa / 2 \right)^2 \tag{3}$$

In Eq. (2), γ denotes the nonlinear coefficient of the waveguide and P_1, P_2 refer to the pumps power. P_0 is also defined as the total pump power ($P_0 = P_1 + P_2$). In Eq. (3), κ represents the

#202294 - $15.00 USD Received 4 Dec 2013; revised 11 Feb 2014; accepted 12 Feb 2014; published 20 Feb 2014

total phase matching between the interacting waves and can be written as the sum of the linear phase mismatch $\Delta\beta$, which is induced by the dispersion of the HNLF, and nonlinear phase mismatch $\Delta\beta_{NL}$, which is related to self-phase and cross-phase modulations of the pumps:

$$\kappa = \Delta\beta + \Delta\beta_{NL} \tag{4}$$

$$\Delta\beta = \beta_2\left[(\Delta\omega_s)^2 - (\Delta\omega_p)^2\right] + \frac{\beta_4}{12}\left[(\Delta\omega_s)^4 - (\Delta\omega_p)^4\right] \tag{5}$$

$$\Delta\beta_{NL} = \gamma(P_1 + P_2) = \gamma P_0 \tag{6}$$

If we denote $\omega_c = (\omega_{P1} + \omega_{P2})/2$ as the central angular frequency of the pumps, then $\Delta\omega_s = \omega_s - \omega_c = (\omega_s - \omega_i)/2$ and $\Delta\omega_p = \omega_{P1} - \omega_c = (\omega_{P1} - \omega_{P2})/2$ are signal and pumps detuning from ω_c, respectively. β_2 and β_4 are also second and fourth order dispersion coefficients of the waveguide at ω_c, respectively. We now introduce $S_{P_0}^G$ the gain sensitivity parameter:

$$S_{P_0}^G = \frac{\left(\partial G / \partial P_0\right)}{G} = \frac{\partial \ln(G)}{\partial P_0} \tag{7}$$

As shown in Eq. (7), this parameter is a measure of how sharp the parametric gain G varies with a small perturbation ∂P_0 from the total pump power P_0. Higher sensitivity will therefore lead to more abrupt change of the signal and idler power. Applying the partial derivative rule, Eq. (7) can be decomposed in two terms, $S_{P_0}^G \partial P_0 = S_{P_1}^G \partial P_1 + S_{P_2}^G \partial P_2$. In Appendix A, we show that $S_{P_{1,2}}^G$ has the following closed form analytical solution:

$$S_{P_n}^G = \frac{1}{P_n} - \frac{\gamma}{g^2}(4\gamma P_{3-n} - \kappa/2) + \frac{L\gamma}{g}(4\gamma P_{3-n} - \kappa/2)\coth(gL) \quad \text{for n=1,2} \tag{8}$$

Equation (8) shows that the sensitivity parameter $S_{P_0}^G$ depends on the linear phase mismatch $\Delta\beta$ through κ. Note that the unit of $S_{P_0}^G$ is Np.W^{-1}. A more practical definition of the gain sensitivity $S_{P_0}^{G_{dB}}$ in dB.W^{-1} units can also be used: $S_{P_0}^{G_{dB}} = \partial \log(G)/\partial P_0 = 10\, S_{P_0}^G / \log(10)$ $\approx 4.343 \times S_{P_0}^G$, which is a measure of the gain variation in dB for 1 watt of total pump variation.

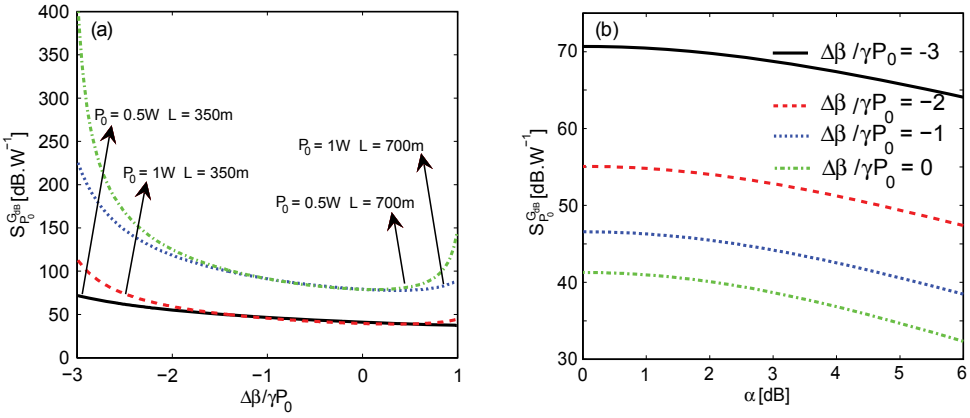

Fig. 1. (a) Gain sensitivity versus normalized phase mismatch term $\Delta\beta/\gamma P_0$ for different pumps total power and HNLF lengths. (b) Gain sensitivity for different linear phase mismatch terms as a function of $\alpha = |P_1/P_2|$.

#202294 - $15.00 USD Received 4 Dec 2013; revised 11 Feb 2014; accepted 12 Feb 2014; published 20 Feb 2014

Figure 1(a) depicts the evolution of the sensitivity as a function of $\Delta\beta/\gamma P_0$ for different values of P_0 and L in a typical HNLF with $\gamma = 15\ \mathrm{W^{-1}.Km^{-1}}$, assuming that the two pumps have identical powers. For equal pumps power $S_{P_0}^{G_{dB}}$ is always strictly positive, which means that if the total pump power decreases, gain decreases by a higher rate. It can therefore be deduced that for a sinusoidal modulation of the pumps with total peak power P_0, narrower pulses will be generated on signal and idler side. For all demonstrated cases in Fig. 1(a), highest sensitivity is obtained for $\Delta\beta = -3\gamma P_0$. Appendix A provides a mathematical proof of this last statement. Figure 1(a) also shows that changing either L or P_0 is not equivalent, as is the case with the parametric gain. Indeed, doubling the HNLF length induces a drastic increase of the sensitivity, whereas doubling P_0 increases the sensitivity only close to the edges of the horizontal axis. Figure 1(b) depicts the influence of unequal pumps powers on sensitivity. In this figure sensitivity is plotted as a function of $\alpha = |P_1/P_2|$ while the total pump power is constant ($P_0 = 0.5$ W). The results show that gain sensitivity decreases as the power imbalance is increased. Note that Eqs. (7) and (8) show a symmetrical influence of P_1 and P_2. It is also verified that Eq. (8) is in good agreement with the FS interaction model for $0.25 \le \alpha \le 1$.

2.2 Generation of optical short pulses in dual-pump FOPA

The study of gain sensitivity to pump power variations showed that a periodic pulse modulation of the pumps $P_1(t)$ and $P_2(t)$ will generate shorter pulses on the signal and the idler side. Moreover, by choosing the appropriate linear phase mismatch $\Delta\beta$, HNLF length L and pumps peak power P_0, a specific gain sensitivity is obtained, which influences the temporal dynamic of the FOPA and hence the pulses that are generated. Since the FOPA is seeded with a continuous wave (CW) signal, a constant optical power remains on the pulse generated on the signal side. Therefore higher extinction ratio will be obtained on the idler side. For this reason, the study is solely focused on pulse generation on the idler side.

In general, the two pumps could be modulated independently with arbitrary modulation format. However in the remainder of this paper we will only focus on the case of sinusoidal intensity modulation. In the most general case, each pump power can be written as:

$$P_n(t) = P_{n0}\cos^2(\pi f_n t + \varphi_n), \quad n = 1,2 \tag{9}$$

Equation (9) infers that by tuning frequencies f_1, f_2 and phases ϕ_1, ϕ_2 along with the gain sensitivity, different repetition rate and pulse widths could be obtained. As an example, if the dual-pump FOPA is designed to have very high sensitivity when the pump peaks coincide in the time domain, there would be significant gain only at that points and therefore the pulses would be generated at a period that is the least common multiple of $1/f_1$ and $1/f_2$. This highlights the potential of dual-pumps FOPA for generating flexible pulse sources in term of repetition rate and pulse width. As this paper is intended to provide a first insight on pulse generation using dual-pump FOPAs, we limit our study to the case where $f_1 = f_2 = f_R$ and $\phi_1 = \phi_2$. Consequently, the period of idler pulses in this case is $1/f_R$. We also consider in the remainder of the paper that P_0 is the total peak power, i.e. $P_0 = P_{10} + P_{20}$. Since it was shown in the previous section that the highest gain sensitivity, hence the shortest pulses are obtained when $P_{10} = P_{20}$, we assume in the following that the pumps powers remain equal and undepleted. Note that the slope of the sensitivity near $\alpha = 0$ dB in Fig. 1(b) is small so that a slight imbalance in the two pumps power can be tolerated.

Injecting Eq. (9) into Eqs. (1)–(3), the duty cycle ($DC = T_{FWHM} \times f_R$) of generated pulses as a function of $\Delta\beta/\gamma P_0$ can be numerically calculated. Note that this is justified as long as the pumps modulation frequency f_R is negligible compared to $\Delta\omega_p$ [14]. The results are depicted in Fig. 2(a) in the range $-3 \le \Delta\beta/\gamma P_0 \le 1$, using the same parameters as in Fig. 1. Figure 2(a) infers that an inverse relation between DC evolution and gain sensitivity evolution as a function of $\Delta\beta$ exists. Indeed, the shortest pulse widths are obtained when $\Delta\beta = -3\gamma P_0$.

#202294 - $15.00 USD Received 4 Dec 2013; revised 11 Feb 2014; accepted 12 Feb 2014; published 20 Feb 2014

Likewise in Fig. 1(a), an inflexion point that shifts towards lower values of $\Delta\beta$ is obtained for higher P_0 and L. For a given set of P_0 and L, the shortest pulses are therefore generated when $\Delta\beta = -3\gamma P_0$. However, contrary to the gain sensitivity, when either P_0 or L is doubled, DC is drastically decreased in the same manner. Figure 2(b) depicts the peak gain as a function of $\Delta\beta/\gamma P_0$. As expected, the highest pulses peak gain is obtained for perfect phase-matching at the pumps peak power ($\Delta\beta = -\gamma P_0$), which corresponds to the case of exponential gain regime whereas the lowest pulses peak gain are obtained in the parabolic regimes where $\Delta\beta = -3\gamma P_0$ or $\Delta\beta = +\gamma P_0$ [5]. Hence, Figs. 2(a) and 2(b) highlight a tradeoff between pulse width and pulse peak power in an analogical manner to the pulse generation in single-pump FOPA [9].

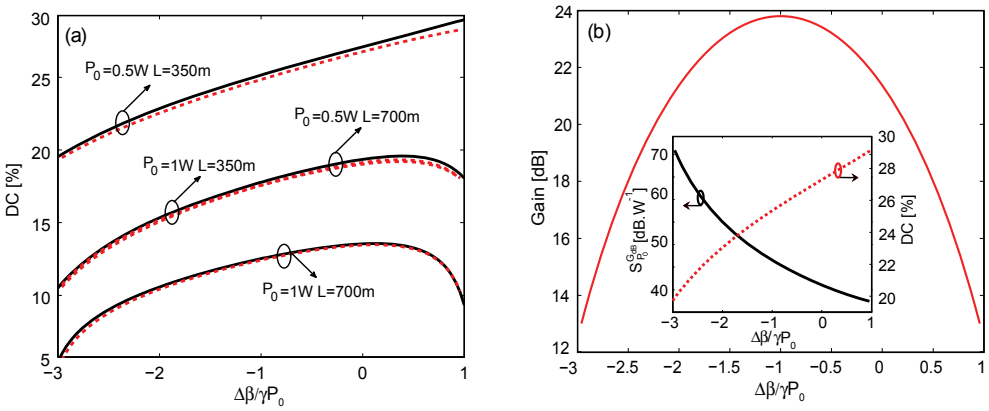

Fig. 2. (a) Idler pulse duty cycle (solid line) defined as $DC = T_{FWHM} \times f_R$ versus normalized phase mismatch term $\Delta\beta/\gamma P_0$ (b) Gain as a function of phase mismatch term $\Delta\beta/\gamma P_0$ for $P_0 = 0.5$ W and $L = 350$ m. The inset shows the inverse relation between $S_{P_0}^G$ and DC.

In order to gain further insight on the behavior of generated pulses and following the discussion on gain sensitivity, it is sufficient to study pulse generation in the vicinity of pumps peak powers and make the following assumption [10]:

$$P(z,t) \approx P_0[1-(\pi f_R t)^2] \tag{10}$$

where $P(z,t)$ is the total pump power. This assumption is valid as long as the generated pulses width is short compared to the repetition rate. Replacing Eq. (10) in Eqs. (1)–(3) leads to closed-form analytical expression for the temporal gain for the cases $\Delta\beta = +\gamma P_0$ ($G_{OUT,1}$), $\Delta\beta = -\gamma P_0$($G_{OUT,-1}$) and $\Delta\beta = -3\gamma P_0$($G_{OUT,-3}$), as derived in Appendix B:

$$G_{out,-3}(t) \simeq (\gamma P_0 L)^2 \operatorname{sinc}^2(\sqrt{3}\gamma P_0 L f_R t) \tag{11}$$

$$G_{out,-1}(t) \simeq \exp(2\gamma P_0 L)/4 \times \exp(-2\gamma P_0 L(\pi f_R t)^2) \tag{12}$$

$$G_{out,1}(t) \simeq (\gamma P_0 L)^2 \operatorname{sinc}^2(\gamma P_0 L f_R t) \tag{13}$$

where $\operatorname{sinc}(x) = \sin(\pi x)/\pi x$. Equations (11)–(13) show that the pulses that are generated in the exponential gain regime exhibit a Gaussian profile, while those that are generated in the parabolic gain regimes exhibit near-sinc shapes. These latter pulses are of particular interest for all-optical generation of Nyquist pulses and time windows [11]. The value of DC in each case can straightforwardly be obtained. Noting from inset in Fig. 2(a) that there is an inverse relation between DC and $S_{P_0}^G$, an empirical relation for DC was obtained using linear regression:

#202294 - $15.00 USD Received 4 Dec 2013; revised 11 Feb 2014; accepted 12 Feb 2014; published 20 Feb 2014

$$DC = \frac{1}{\pi}\sqrt{\frac{2\ln 2}{\gamma P_0 L}} + \frac{0.62}{\sqrt{P_0}}\left(\frac{1}{\ln\left(S_{P_0}^{G}\right)} - \frac{1}{\ln\left(2\gamma L \coth(\gamma P_0 L)\right)}\right) \tag{14}$$

Equation (14) is plotted in dashed line in Fig. 2(a) and shows a good agreement with calculated duty cycles (solid line). Figures 3(a) and 3(b) illustrate the evolution of the generated pulse shapes as a function of $\Delta\beta/\gamma P_0$ for L = 350 m and P_0 = 0.5 W. It is verified that for $\Delta\beta = -\gamma P_0$ and $\Delta\beta = -3\gamma P_0$ the derived shapes fit well with the calculated shapes. In the case $\Delta\beta = +\gamma P_0$, the DC is accounted for by Eq. (13) but the sinc shape is not retrieved. This is due to the fact that when the pulse width is too large, Eq. (13) does not fit the generated pulse over the entire period. It can be verified that for higher L or P_0, the formula fits the generated pulse. Figure 3(b) and Eqs. (11)–(13) show that in order to generate near-sinc pulses, it is preferable to operate at $\Delta\beta = -3\gamma P_0$.

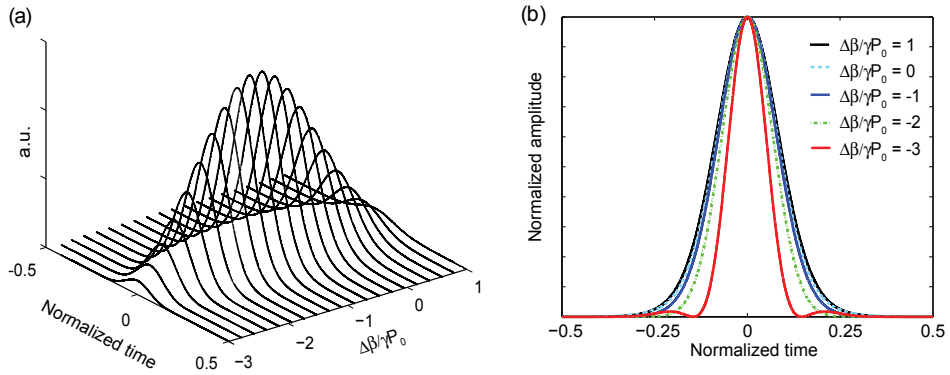

Fig. 3. (a) Idler pulse shapes over one period as a function of $\Delta\beta/\gamma P_0$ (b) Normalized intensity of idler pulses over one period for different phase matching condition.

2.3 Generation of identical shaped pulses over a wide bandwidth

The previous section showed that depending on the linear phase mismatch $\Delta\beta$, different pulse shapes can be obtained. In this section, it will be shown that it is possible to bound $\Delta\beta$ over a wide bandwidth and thus generate uniform pulse shapes over that bandwidth. This is a significant advantage of dual-pump FOPAs compared to single-pump FOPAs where the pulse shape depends on the signal detuning from the pump frequency. Note that this was demonstrated for CW dual-pump FOPA operating in the exponential gain regime [15]. The novelty of this work is to show that such bounding can be extended to any $\Delta\beta$ in the interval $[-3\gamma P_0, \gamma P_0]$.

Consider $m \in [-3,1]$. When $\beta_2 \cdot \beta_4 < 0$, $\Delta\beta$ can be expressed in terms of a Chebyshev polynomial as shown in Eq. (15):

$$\frac{\Delta\beta}{\gamma P_0} = m + \rho T_4\left(\frac{\Delta\omega_s}{\Delta\omega_t}\right) \tag{15}$$

where $T_4(x) = 8x^4 - 8x^2 + 1$ is the fourth order Chebyshev polynomial, ρ is the relative ripple in $\Delta\beta$, and $\Delta\omega_t$ denotes half the bandwidth over which the ripple remains between the Chebyshev extrema [15]. Using Eq. (5), the two sides of Eq. (15) are identical for any $\Delta\omega_s$ if we have:

#202294 - $15.00 USD Received 4 Dec 2013; revised 11 Feb 2014; accepted 12 Feb 2014; published 20 Feb 2014

$$\Delta\omega_t = \sqrt{-12\frac{\beta_2}{\beta_4}} \tag{16a}$$

$$\rho = \frac{3}{2}\frac{\beta_2^2}{\beta_4\gamma P_0} \tag{16b}$$

$$\left(\frac{\beta_4}{12\gamma P_0}\right)\left(\Delta\omega_p^4\right)+\left(\frac{\beta_2}{\gamma P_0}\right)\left(\Delta\omega_p\right)^2+(\rho+m)=0 \tag{16c}$$

when the conditions given in Eqs. (16a)–(16c) are met, the normalized phase mismatch is bound to m in the $2\Delta\omega_t$ frequency range with ripple amplitude of ρ. It is important to note that Eq. (16c) is satisfied if and only if $\mathrm{sgn}(\beta_4)m < |\rho|$. Therefore depending on the sign of β_4 and the value of m, four different types of operating regions can be determined.

Type (*i*) corresponds to $\mathrm{sgn}(\beta_4) > 0$, $m \in [-3,0]$ and type (*ii*) to $\mathrm{sgn}(\beta_4) < 0$, $m \in [0,1]$, where $\mathrm{sgn}(\beta_4)m$ is always negative and hence readily verifies the condition for any set of m and ρ. In these cases, m and ρ can be arbitrary chosen. In order to have $|\rho| < |m|$, (i.e. ripples are small compared to m) it is necessary to set the central frequency of the pumps such that:

$$\beta_2 = -\frac{\beta_4\Delta\omega_p^2}{3}\left[1-\left(\frac{1}{2}-\frac{6m\gamma P_0}{\beta_4\Delta\omega_p^4}\right)^{1/2}\right] \tag{17}$$

from which we obtain

$$\Delta\omega_t = 2\Delta\omega_p\left(1-\left\{\frac{1}{2}\left[1+\left(\frac{\Delta\omega_4}{\Delta\omega_p}\right)^4\right]\right\}^{1/2}\right)^{1/2} \tag{18}$$

where $\Delta\omega_4 = (|12m\gamma P_0/\beta_4|)^{1/4}$. Equations (17) and (18) reveal that as $\Delta\omega_p$ ranges from $\Delta\omega_4$ to $2^{3/4}\,\Delta\omega_4$, $\Delta\omega_t$ ranges from 0 to $\Delta\omega_p$ while $|\rho|$ ranges from 0 to $|m|$. As a result, there is a trade-off between the bandwidth of the pulses and the ripples of $\Delta\beta$, which will induce fluctuations on the pulses width (or *DC*) and peak power.

Type (*iii*) corresponds to $\mathrm{sgn}(\beta_4) > 0$ and $m \in [0,1]$, while in type (*iv*), $\mathrm{sgn}(\beta_4) < 0$ and $m \in [-3,0]$. These two operating conditions lead to $|m| < |\rho|$, indicating that the minimum achievable ripple is higher than the absolute value of m. Therefore, one must use the operating conditions described in type (*i*) or (*ii*) in order to confine the linear phase mismatch with low ripples. This study therefore shows that fibers with positive dispersion curvature (β_4) are advantageous for generating Gaussian or sinc shaped pulses over a wide bandwidth.

Figure 4(a) describes how $\Delta\beta/\gamma P_0$ ripples influence the ripples of *DC* in a type (*i*) operating condition. As the normalized phase mismatch is confined between $m-\rho$ and $m+\rho$ over $2\Delta\omega_t$, the *DC* of the generated pulses is also bound over that same bandwidth. The amplitude of the oscillations of *DC* is determined by ρ and the slope of the *DC* curve versus $\Delta\beta/\gamma P_0$ at the operating point m.

#202294 - $15.00 USD Received 4 Dec 2013; revised 11 Feb 2014; accepted 12 Feb 2014; published 20 Feb 2014

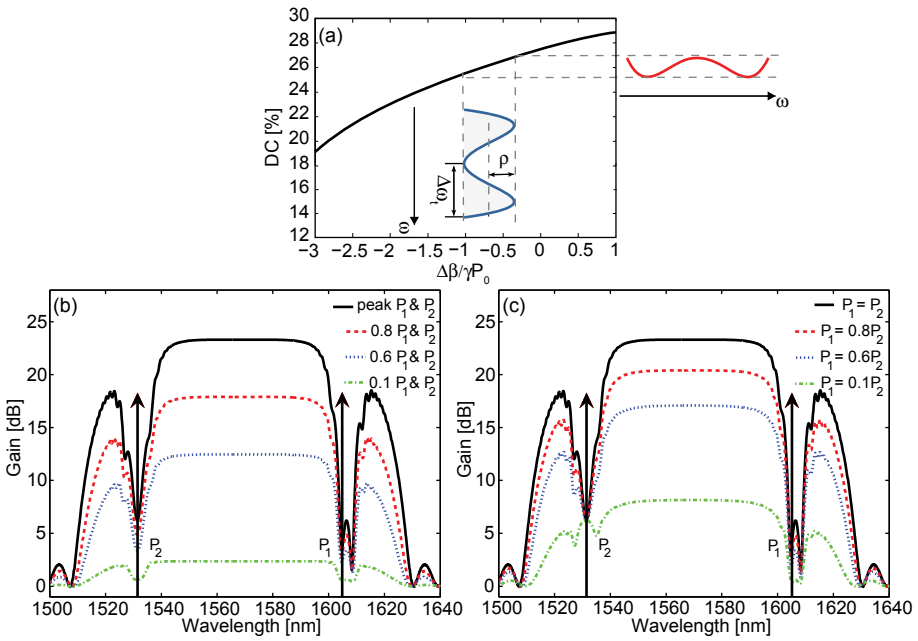

Fig. 4. (a) Basic principle of pulse generation in dual-pump FOPA. As $\Delta\beta/\gamma P_0$ is bound to m with a ripple ρ, the DC of generated pulses follows a similar trend in frequency. Instantaneous dual-pump FOPA gain spectra (b) two synchronously modulated pumps (c) one modulated and one CW pump. The peak power of each pump is $P_0/2 = 0.25$W.

To illustrate uniform pulse generation over a wide bandwidth in a dual-pump FOPA, we have depicted in Fig. 4(b) the gain spectra of a typical dual-pump FOPA when both P_1 and P_2 are varied simultaneously and in Fig. 4(c) when either P_1 or P_2 is varied, the other being fixed at $P_0/2$. This latter case that was experimentally studied in [16] is more cost effective as it requires only one pump to be modulated. The nonlinear coefficient of the HNLF is the same as in Fig. 1 while the dispersion parameters are $\beta_2 = -5.8 \times 10^{-31}$ s^{2}m^{-1}, $\beta_3 = 3.6 \times 10^{-41}$ s^{3}m^{-1} and $\beta_4 = 5 \times 10^{-56}$ s^{4}m^{-1} so as to achieve $m = -0.28$ and $\rho = 0.001$. The spectra were calculated using the FS model. In all cases, the gain is decreased by a substantial amount over the whole bandwidth when at least one pump is slightly decreased. When both pumps are simultaneously decreased by 20%, Fig. 4(b) shows that the gain drops by more than 7 dB over 40 nm in the inner band of the two pumps, while remaining flat. In Fig. 4(c), when one of the two pumps is decreased by 20%, the gain drops by more than 3 dB over the same bandwidth. Indeed in [16], it was shown that for Gaussian pulses; the full width half maximum is increased by a factor of $\sqrt{2}$ when only one of the pumps is modulated compared to the case of two synchronous modulated pumps. Note that apart from the region close to the pumps, the behavior is similar if either P_1 or P_2 is decreased, in agreement with Eq. (8) where the TS model was used. Therefore, modulating either of the pumps will induce the generation of the same pulses over the region where the TS model holds valid. Although more complex experimentally, modulating simultaneously both pumps induces the generation of shorter pulses than modulating one of the pumps.

#202294 - $15.00 USD Received 4 Dec 2013; revised 11 Feb 2014; accepted 12 Feb 2014; published 20 Feb 2014

3. Dual-pump FOPA pulse generation experiment

3.1 Experimental setup

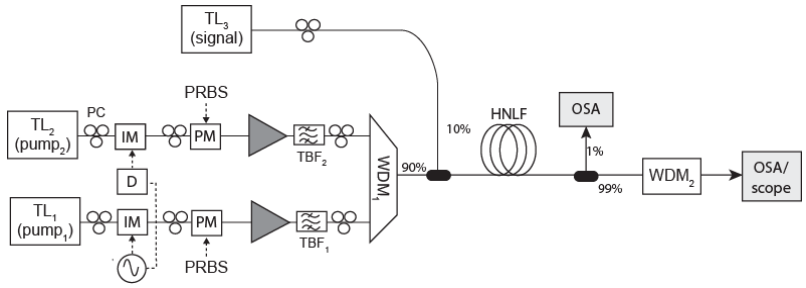

Fig. 5. Experimental setup of pulse generation in dual-pump FOPA. TL: tunable laser; IM: intensity modulator; PM: phase modulator; PC:polarization controller; TBF: tunable bandpass filter; WDM: wavelength division multiplexer; OSA: optical spectrum analyzer.

The experimental setup used to test the theory is depicted in Fig. 5. Two tunable high signal to noise ratio (SNR) CW external cavity lasers (TL_1 and TL_2) are used as FOPA pumps. The lasers are intensity modulated by a sinusoidal wave at 5 GHz. A tunable RF delay line is inserted to ensure the synchronization of the two pumps. Both pumps are phase modulated by a 2.5 GHz pseudo random bit sequence (PRBS) in order to suppress the stimulated Brillouin scattering (SBS). The delay of each PRBS source is tuned so that each phase jump occurs during the dip of the sinusoidal intensity modulated pump [10]. Using an out-of-phase modulation scheme, it is possible to cancel any pump phase modulation induced distortion [17, 18]. However, because of lack of equipment we were not able to realize this scheme. The pumps are amplified and filtered to suppress amplified spontaneous emission (ASE) and coupled with a wavelength division multiplexer (WDM). An additional tunable CW laser (TL_3) acting as a signal source is combined through a 10/90 coupler. The signal could be swept across both C and L bands. The three optical waves are then launched into a 350 m long HNLF with nonlinearity coefficient $\gamma = 15\ W^{-1}.Km^{-1}$ and zero dispersion wavelength (ZDW) $\lambda_0 = 1568.9$ nm. The third and fourth order dispersion parameters of the fiber are $\beta_3 = 3.6 \times 10^{-41}\ s^3m^{-1}$ and $\beta_4 = 5 \times 10^{-56}\ s^4m^{-1}$, respectively. The power of injected signal during the experiment is kept low enough to avoid pump depletion and multiple FWM process. At the output of the fiber the parametric process is monitored through a 1% tap on an optical spectrum analyzer (OSA). Finally a WDM and a tunable filter are employed to separate the generated idler from the high power pumps and signal. The temporal and spectral characteristics of the generated pulsed idler are then monitored on an OSA and a 50 GHz oscilloscope covering the C and L band.

3.2 Results

Two cases corresponding to different operating conditions described in section 2.3 were examined in order to verify the theory. In the first case the pumps are set at $\lambda_1 = 1532.3$ nm and $\lambda_2 = 1608.3$ nm leading to $\beta_2 = -1.5 \times 10^{-29}\ s^2m^{-1}$, which corresponds to $m = 0.35$ with high ripples amplitude of $\rho = 0.55$. In the second case λ_2 is adjusted in order to provide a phase matching that is bound with minimum ripple. The second pump wavelength was set at $\lambda_2 = 1607.2$ nm, for which the dispersion $\beta_2 = -5.8 \times 10^{-31}\ s^2m^{-1}$ led to $m = -0.28$ and $\rho = 0.001$ over $2\Delta\omega_i/2\pi = 4.9$ THz. Table 1 summarizes these settings. Note that because higher ripples are tolerated in case 1, the bandwidth is also larger compared to the second case. Also, due to the positive β_4 of the fiber under test, our experiments were limited to the operating region of type (*iii*) for case 1 and type (*i*) for case 2.

#202294 - $15.00 USD Received 4 Dec 2013; revised 11 Feb 2014; accepted 12 Feb 2014; published 20 Feb 2014

Table 1. Summary of the Settings and Parameters for the Three Experimental Cases Studied

	Pump 1	Pump 2	β_2 (s^2m^{-1})	m	$\lvert\rho\rvert$	$2\Delta\omega_t/2\pi$
Case 1	532.3 nm	1608.3 nm	-1.5×10^{-29}	0.35	0.55	Non applicable
Case 2	532.3 nm	1607.2 nm	-5.8×10^{-31}	−0.28	0.001	4.9 THz

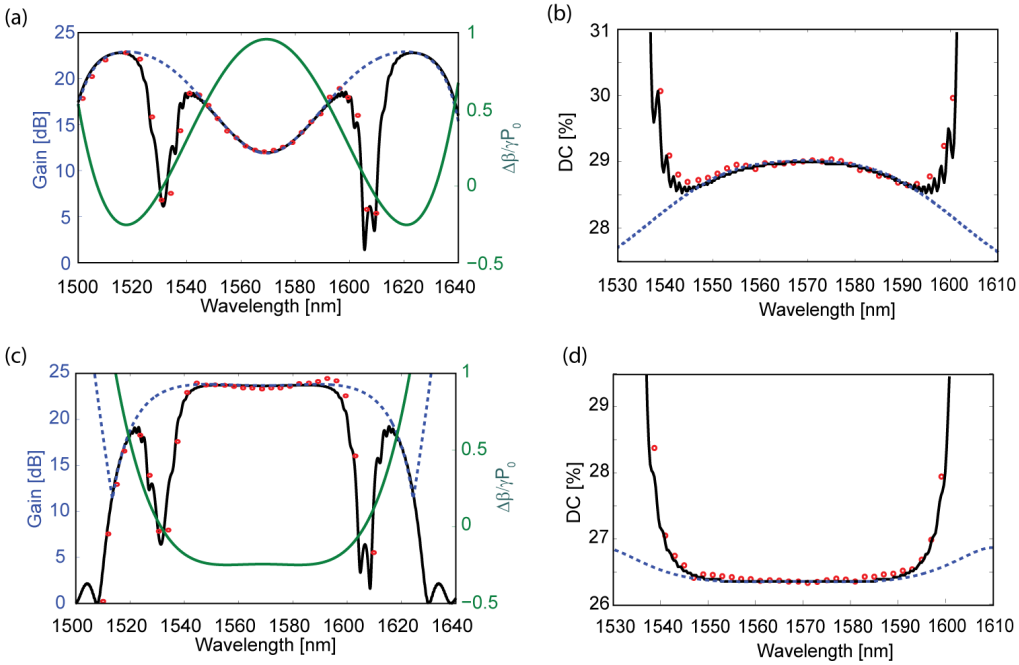

Fig. 6. Results of pulse-width behavior in dual-pump FOPA for case 1 and case 2 parameters. (a) and (c): experimental (dot) and theoretical gain spectrum obtained from TS (dash line) and FS (solid line) interaction model as well as normalized phase mismatch for case 1 and 2, respectively. (b) and (d): experimental (dot) *DC* values along with theoretical results derived from TS (dash line) and FS (solid line) interaction model case 1 and 2, respectively.

For both cases experimental and theoretical gain spectra are plotted in Figs. 6(a) and 6(c) along with the normalized phase mismatch terms derived from the theory. The corresponding experimental *DC* measurements are shown in Figs. 6(b) and 6(d). Both TS and FS interaction models are employed to obtain theoretical data in all figures. Figures 6(a) and 6(b) show that in case 1, $\Delta\beta/\gamma P_0$ varies significantly between 0.45 to 0.95 over the 54 nm bandwidth between the pumps, leading to fluctuations of over 0.005 of the pulses duty cycle, or 1.72% of the averaged duty cycle. In the second case depicted in Figs. 6(c) and 6(d), low-ripple of the linear phase mismatch is experimentally demonstrated over 40 nm. Flat gain close to 23 dB and flat linear phase mismatch of $-0.28\gamma P_0$ are simultaneously achieved. The measured *DC* value of the generated pulses remains close to 0.265 over a 40 nm wavelength range with less than 0.04% variations. In both cases an increase of *DC* in the vicinity of the pumps is observed, which is correctly predicted by the FS interaction model and is therefore due to the sidebands generated in the outer band of the two pumps.

The variations of the idler pulses peak power follow the same trend as the gain spectrum. Figures 7(a) and 7(b) show the experimental averaged pulse shape evolution with idler wavelength for the two cases. Figures 7(b) and 6(d) demonstrate that a truly identical pulse generation both in terms of *DC* and peak power is realized when the phase mismatch is correctly bound according to Eqs. (16)–(18). In Fig. 7(c) the actual idler pulses and their averaged profiles are depicted when $\Delta\beta/\gamma P_0 = 0.9$, which corresponds to an idler wavelength close to 1570 nm in case 1, and when $\Delta\beta/\gamma P_0 = -0.28$, which corresponds to an idler

#202294 - $15.00 USD Received 4 Dec 2013; revised 11 Feb 2014; accepted 12 Feb 2014; published 20 Feb 2014

wavelength anywhere between 1548 nm and 1588 nm in case 2. The difference in pulse width between these two pulses is 5 ps, in agreement with theoretical predictions.

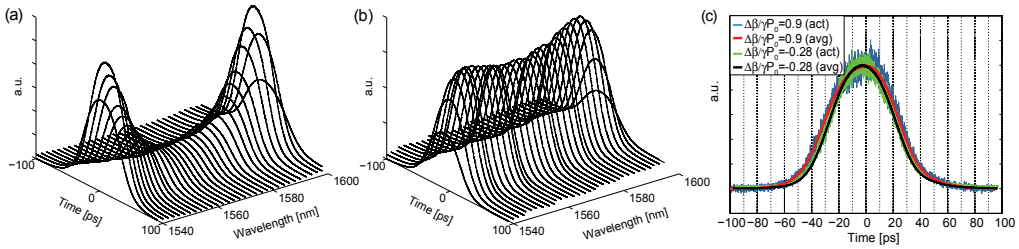

Fig. 7. (a) and (b) depict average pulse shape evolution with idler wavelength respectively regarding the first and second phase matching condition described in Table 1. (c) Actual (act) and averaged (avg) pulse shape for $\Delta\beta/\gamma P_0 = 0.9$ in the first case and for $\Delta\beta/\gamma P_0 = -0.28$ in the second case.

4. Discussion and conclusion

We have studied the theory of pulse generation in dual-pump FOPA for the first time to the best of our knowledge. Introducing the gain sensitivity parameter, the duty cycle (*DC*) or pulse width of the generated pulses has been shown to depend on the total input power P_0, fiber length L, and the linear phase matching between the interacting waves. An analytical formula was derived for the *DC* of the generated pulses. The gain sensitivity could also be used to investigate other properties of dual-pump FOPAs such as pumps relative intensity noise (RIN) transfer, or multicasting with data-modulated pump.

It was shown that it is possible in dual-pump FOPA to bound the linear phase mismatch term over a wide bandwidth to any value between $-3\gamma P_0$ and γP_0 and hence to achieve a constant peak gain and *DC* over that bandwidth. Theory was experimentally verified by generating uniform pulses at 5 GHz repetition rate over 40 nm of bandwidth with less than 0.04% *DC* fluctuations. The setup was limited by the 50 GHz electrical bandwidth of the C + L oscilloscope and could easily be extended to higher repetition rate. Note that pulse generation based on single-pump FOPA has been shown at repetition rates up to 40 GHz [14, 19]. The good agreement between theoretical and experimental results shows that the impact of walk-off between the interacting waves is negligible. However at higher pump repetition rate, a dedicated study of walk-off is needed to adequately comprehend how the pulse shape would be affected. One solution for reducing walk-off is to decrease the HNLF length. Note however that the pumps powers should be increased accordingly while the pumps position should be recalculated in order to obtain uniform operation over a wide bandwidth.

It worth to note that the generated pulses amplitude exhibit a phase that is equal to $\beta_3\Delta\omega_s^3 L/6 + \gamma P_0\cos^2(\pi f_R t)L$ [5]. This expression shows that β_3 is responsible for walk-off [20] whereas $\gamma P_0\cos^2(\pi f_R t)L$ that originates from cross-phase modulation, induces a chirp on the generated pulse. Thus, the generated pulses are not transform-limited. Note that in analogy with the single-pump FOPA case, Gaussian pulses could be shortened by using a dispersive medium to reach a transform-limited pulse, whereas sinc-like pulse chirp compensation is more challenging [11]. In our experiment, the SNR of the generated pulses in the case of wideband uniform pulse generation was measured at 27 dB. The focus of this study was to demonstrate uniform pulse generation over a wide bandwidth; however by improving the optical signal to noise ratio (OSNR) of the pumps, using for example narrower filters and/or a two-stage amplifying module for the pumps, it could be possible to further improve the pulses SNR [21, 22].

The limitations of the EDFAs in terms of bandwidth prevented a wideband linear phase mismatch bounding close to $m = -1$ where the highest peak power can be achieved. Also, by further increasing the distance between the pumps, it could be possible to achieve $m = -3$ over a wide bandwidth and hence generate near-Nyquist pulses over a broad bandwidth.

#202294 - $15.00 USD Received 4 Dec 2013; revised 11 Feb 2014; accepted 12 Feb 2014; published 20 Feb 2014

Efficient wavelength conversion techniques to expand the distance between the two sinusoidally modulated pumps can alleviate these limitations [23]. As an example, using the same parameters as in the experiment, generation of uniform Gaussian and sinc shape pulses requires the pumps to be 11 THz and 15 THz apart, respectively. Thus, a Nyquist sampler over 6.8 THz (56 nm), which could sample at the Nyquist rate without inter symbol interference (ISI) could be demonstrated.

Finally, generation of pulses with dual-pump FOPAs offer the unique flexibility of modulating each pump independently, thus generating a wide variety of pulse and time window shapes. In [16], we showed that modulating one of the two pumps is sufficient to generate uniform pulses with dual-pump FOPA. However the corresponding pulse width is wider by a factor of $\sqrt{2}$ when compared to the two synchronous modulated pumps. The possibility of modulating the pumps at different frequencies could also pave the way for pulse sources where the width and repetition rate of the pulses could be tuned independently. This scheme could also be used to compress in the time domain, WDM pulses carrying data for subsequent optical time division multiplexing, thus allowing transparent modification of the network granularity.

Appendix

A. Gain sensitivity

To obtain $S_{P_1}^G$ we first find the derivative of G with respect to P_1:

$$\frac{\partial G}{\partial P_1} = \frac{\partial}{\partial P_1}\left(\frac{r}{g}\sin \mathrm{h}(gL)\right)^2 = \frac{\partial}{\partial P_1}\left(\frac{r}{g}\right)^2 \sin \mathrm{h}^2(gL) + \left(\frac{r}{g}\right)^2 \frac{\partial}{\partial P_1}\sin \mathrm{h}^2(gL) \qquad (19)$$

To proceed with Eq. (19) we take the partial derivative of Eq. (3) with respect to P_1 to obtain $dg/dP_1 = r(2\gamma P_2 - \kappa/4)/g$. Therefore Eq. (19) can be calculated as:

$$\frac{\partial G}{\partial P_1} = 2\frac{r^2}{g^2}\sin \mathrm{h}^2(gL)\left(\frac{1}{2P_1} - \frac{\gamma}{g}(2P_2 - \kappa/4) + \frac{\gamma L}{g}(2P_2 - \kappa/4)\coth(gL)\right) \qquad (20)$$

According to the definition of Eq. (8) and using Eqs. (1a) and (20), the gain sensitivity is:

$$S_{P_1}^G = \frac{\left(\partial G \big/ \partial P_1\right)}{G} = \frac{1}{P_1} - \frac{\gamma}{g^2}(4\gamma P_2 - \kappa/2) + \frac{\gamma L}{g}(4\gamma P_2 - \kappa/2)\coth(gL) \qquad (21)$$

calculating the expression for $S_{P_2}^G$ leads to a similar expression as Eq. (21) except that P_1 is replaced with P_2 and vice versa.

Equation (21) has a determinate value for any phase matching condition in the rage $-3 < \Delta\beta/\gamma P_0 < 1$. However, when $\Delta\beta/\gamma P_0 = -3,1$ it takes an indeterminate form of 0/0. To evaluate $S_{P_1}^G$ when $\Delta\beta\gamma P_0 \to -3,1$ which leads to $g \to 0$, one can replace $\coth(gL)$ with its Laurant series expansion in the range $0 < |gL| < \pi$ i.e. $\coth(gL) = 1/gL + gL/3 + O((gL)^3)$. Therefore we can rewrite Eq. (21) as:

$$S_{P_1}^G = \frac{1}{P_1} + (4\gamma^2 P_2 - \kappa\gamma/2) \times \left(\frac{L^2}{3} + \frac{L}{g}O(gL)^3\right), \quad 0 < |gL| < \pi \qquad (22)$$

from which we obtain

#202294 - $15.00 USD Received 4 Dec 2013; revised 11 Feb 2014; accepted 12 Feb 2014; published 20 Feb 2014

$$\lim_{\Delta\beta/\gamma P_0 \to -3} S_{P_1}^G = \frac{1}{P_1} + \frac{\gamma^2 L^2 (4P_2 + P_0)}{3}, \quad \lim_{\Delta\beta/\gamma P_0 \to 1} S_{P_1}^G = \frac{1}{P_1} + \frac{\gamma^2 L^2 (4P_2 - P_0)}{3} \tag{23}$$

It worth to note that the value of gain sensitivity at $\Delta\beta/\gamma P_0 = -3$ is the supermum of $S_{P_1}^G$. Accordingly, based on the definition of gain sensitivity it is assured that the generated pulses experience lowest *DC* when operating at $\Delta\beta/\gamma P_0 = -3$. To confirm this theory we employ the approximation of Eq. (21) when $|gL| > \pi$ where:

$$S_{P_1}^G = \frac{1}{P_1} + (4\gamma^2 P_2 - \kappa\gamma/2) \times \left(\frac{L^2}{gL} - \frac{1}{g^2} \right), \quad |gL| > \pi \tag{24}$$

Equation (24) can be inspected together with Eq. (22) to show that the gain sensitivity at $\Delta\beta/\gamma P_0 = -3$ is an upper bound for $S_{P_1}^G$. In fact the second expression at the right hand side of both equations consists of two multiplied terms. In the one hand the first term $(4\gamma^2 P_2 - \kappa\gamma/2)$ is maximized at $\Delta\beta/\gamma P_0 = -3$ in the range $-3 \le \Delta\beta/\gamma P_0 \le 1$. On the other hand the second term takes the maximum value $L^2/3$ for all $|gL| > 0$. As a result $1/P_1 + \gamma^2 L^2 (4P_2 + P_0)/3$ which is also derived is Eq. (23) is the supermum of $S_{P_1}^G$.

B. Pulse shape

In this section we derive expressions for the output generated optical pulses at different values of $\Delta\beta/\gamma P_0 = -3, -1, 1$. Since the pumps are sinosuidally modulated, according to Eqs. (2)–(4) we can write

$$r(t) = \gamma P_0 \cos^2(\pi f_R t) \tag{25}$$

$$\kappa(t) = \Delta\beta + \gamma P_0 \cos^2(\pi f_R t) \tag{26}$$

Considering Eq. (26), we can obtain the values of $\kappa(t)$ at $\Delta\beta/\gamma P_0 = m$ as follows:

$$\Delta\beta / \gamma P_0 = m \Rightarrow \kappa(t) = \gamma P_0 (m + \cos^2(\pi f_R t)) \tag{27}$$

Based on Eqs. (25)–(27), Eq. (3) and making the assumption mentioned in section 2.2 (pump expression can be replaced with its development to the second order in *t*), one can derive the approximated *g* as follow:

$$\Delta\beta / \gamma P_0 = -3 : g \simeq j\sqrt{3}\gamma P_0 \left|\sin(\pi f_R t)\right| \simeq j\sqrt{3}\pi\gamma P_0 f_R t \tag{28a}$$

$$\Delta\beta / \gamma P_0 = -1 : g \simeq \gamma P_0 (1 - \sin^2(\pi f_R t))^{1/2} \simeq \gamma P_0 (1 - (\pi f_R t)^2) \tag{28b}$$

$$\Delta\beta / \gamma P_0 = 1 : g \simeq j\gamma P_0 \left|\sin(\pi f_R t)\right| \simeq j\pi\gamma P_0 f_R t \tag{28c}$$

From Eqs. (28a)–(28c) and Eqs. (1)–(3), we can write the following expression for the output optical generated pulses:

$$\Delta\beta / \gamma P_0 = -3 : P_{out}(t) \simeq P_s (\gamma P_0 L)^2 \sin c^2 (\sqrt{3}\gamma P_0 L f_R t) \tag{29a}$$

$$\Delta\beta / \gamma P_0 = -1 : P_{out}(t) \simeq P_s \exp(2\gamma P_0 L)/4 \times \exp(-2\gamma P_0 L (\pi f_R t)^2) \tag{29b}$$

$$\Delta\beta / \gamma P_0 = 1 : P_{out}(t) \simeq P_s (\gamma P_0 L)^2 \sin c^2 (\gamma P_0 L f_R t) \tag{29c}$$

#202294 - $15.00 USD Received 4 Dec 2013; revised 11 Feb 2014; accepted 12 Feb 2014; published 20 Feb 2014